

Exponential Signal Reconstruction with Deep Hankel Matrix Factorization

Yihui Huang[†], Jinkui Zhao[†], Zi Wang, Di Guo, Xiaobo Qu^{*}

Abstract—Exponential is a basic signal form, and how to fast acquire this signal is one of the fundamental problems and frontiers in signal processing. To achieve this goal, partial data may be acquired but result in the severe artifacts in its spectrum, which is the Fourier transform of exponentials. Thus, reliable spectrum reconstruction is highly expected in the fast sampling in many applications, such as chemistry, biology, and medical imaging. In this work, we propose a deep learning method whose neural network structure is designed by unrolling the iterative process in the model-based state-of-the-art exponentials reconstruction method with low-rank Hankel matrix factorization. With the experiments on synthetic data and realistic biological magnetic resonance signals, we demonstrate that the new method yields much lower reconstruction errors and preserves the low-intensity signals much better.

Index Terms—exponential signal, deep learning, Hankel matrix, reconstruction, low rank

I. INTRODUCTION

EXPONENTIAL function is a basic signal form in signal processing. In many practical applications, signals can be approximated by the superposition of a few numbers of exponential functions. Examples include antenna signals in telecommunication [1-3], images in fluorescence microscopy [4], analog-to-digital conversion in electronic systems [5], signal functions in the theory of the finite rate of innovation [6], and time-domain signals in biological Nuclear Magnetic Resonance (NMR) spectroscopy [7-11]. Thus, achieving high-quality recovery of the exponential signals has great significance. The signal of interest is modeled as the sum of exponentials as follows:

This work was supported in part by the National Natural Science Foundation of China (61971361, 61871341, 61811530021 and U1632274), the National Key R&D Program of China (2017YFC0108703), the Natural Science Foundation of Fujian Province of China (2018J06018), the Fundamental Research Funds for the Central Universities (20720180056 and 20720200065), and Xiamen University Nanqiang Outstanding Talents Program. ([†]Equal Contributions, ^{*} Corresponding author)

Yihui Huang, Jinkui Zhao, Zi Wang, and Xiaobo Qu are with the Department of Electronic Science, Fujian Provincial Key Laboratory of Plasma and Magnetic Resonance, Xiamen University, Xiamen, China (e-mail: quxiaobo@xmu.edu.cn).

Di Guo is with the School of Computer and Information Engineering, Xiamen University of Technology, Xiamen, China.

$$x(n\Delta t) = \sum_{j=1}^J (A_j e^{i\phi_j}) e^{-\frac{n\Delta t}{\tau_j}} e^{i2\pi f_j n\Delta t}, \quad (1)$$

where $f_j \in [0,1)$ is the normalized frequency, $\phi_j \in [0,2\pi)$ is the phase, $A_j \in \mathbb{R}_+$ is the amplitude, $\tau_j \in \mathbb{R}_+$ is the damping factor, J is the number of exponentials, $j=1,\dots,J$, and Δt is the sampling interval, n is the index of data points in the time domain and $n=1,2,\dots,N$ means the fully sampling. Accordingly, the sampled data can be represented with a vector $\mathbf{x} = [x_1, \dots, x_N]^T \in \mathbb{C}^N$. By performing the Fourier transform \mathbf{F} on \mathbf{x} , one can obtain a full spectrum $\mathbf{F}\mathbf{x}$.

Reconstruction and fast sampling of exponentials is one of the frontier and important problems in signal processing [6, 7, 9-15]. To enable fast samplings, the main approach is to acquire the non-uniformly sampled time domain data $\mathbf{y} = \mathbf{U}\mathbf{x}$ where $\mathbf{U} \in \mathbb{R}^{M \times N}$ denotes the undersampling operator with $M < N$. As the system is underdetermined, one has to introduce some priors to recover the signal \mathbf{x} from \mathbf{y} . For instance, in biological NMR spectroscopy [7], exponential signal reconstruction from the undersampled data has enabled the acceleration factor of 4 to 10 in fast sampling, which significantly reduces the data acquisition time [7, 16-21].

To reconstruct exponentials \mathbf{x} from the undersampled data \mathbf{y} , there are two main model-based approaches, which explore the sparsity of $\mathbf{F}\mathbf{x}$ in the frequency domain and low rankness of \mathbf{x} in the time domain. Without particularly considering the damping factor, i.e., the signal decay, the former has been evidenced powerful in conventional compressed sensing [22] and state-of-the-art total variation or atomic norm methods [23].

The sparsity of the spectrum $\mathbf{F}\mathbf{x}$, however, may not be satisfied for a fast decaying exponential, as broad spectral peaks (Fig. 1) may be introduced with a damping factor [7]. Thus, researchers tend mathematical property in another domain, the time domain, of \mathbf{x} . By converting the \mathbf{x} into a Hankel matrix, the matrix rank will be equal to the number of exponentials [7]. Thus, the damped exponential will be strictly low rank in the Hankel matrix, assuming that the number of exponentials is much smaller than the number of data points N [7, 13, 14, 24-27]. Then, \mathbf{x} can be recovered by enforcing the low rankness of the Hankel matrix [7]. This approach is called Low-Rank Hankel Matrix Completion (LRHMC) [7, 13, 14, 24-27].

A fast algorithm remains challenging to LRHMC once the faithful reconstruction is achieved. Since the rank minimization problem was NP-hard, some approaches utilized the nuclear

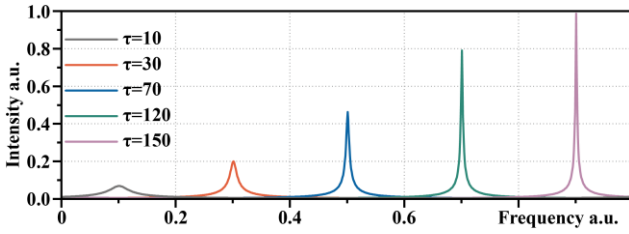


Fig. 1. A synthetic spectrum with low-intensity peaks that are introduced by small damping factors. Note: Five peaks are generated with the same amplitudes and phases in (1), and frequencies are set from 0.1 to 0.9. The corresponding damping factors from the left to right peaks are 10, 30, 70, 120 and 150, respectively. Thus, smaller damping factor leads to broader and lower peaks.

norm to relax it into a convex optimization problem [7, 14, 26, 28]. These approaches lead to the faithful reconstruction of exponentials and high fidelity spectra in applications, such as fast biological NMR [7]. However, time-consuming singular Value Decomposition (SVD) was commonly used to minimize the nuclear norm [29] which may take minutes or even hours in reconstruction [7]. Although matrix factorizations [9, 11, 30, 31] were proposed to avoid SVD, the computational time still needs to be reduced due to many iterations in these model-based optimization algorithms.

Inspired by the great achievement of deep learning (DL)[32, 33], a proof-of-concept of exponentials reconstruction with DL was proposed and applied to fast NMR with undersampling [12]. It showed that the neural network training can be achieved using solely synthetic exponential signals, which lifted the prohibiting demand for a large volume of realistic biological training data that are expensive or even hardly acquired [12, 34]. Besides, ultrafast computation was provided as the traditional iterative reconstruction is reduced to a forward process once the network has been trained on graphics processing units (GPUs) with parallel computing.

Nevertheless, from the perspective of applications, the distortion for reconstruction on low-intensity exponentials (or spectral peaks) remains a problem in DL [12]. From the standpoint of method, this approach is lack of interpretability, such as the guidance to design the network structure. A possible solution to this problem is to introduce a well-established model-based optimization method to guide network design [33, 35, 36].

In this work, we propose a DL neural network to recover exponentials by unfolding the established model-based low-rank Hankel reconstruction algorithm [7, 9]. Our design starts from constraining the low rank property of the Hankel matrix which is arranged from exponential signals and adopts matrix factorization-based LRHMC [7, 9] which are SVD-free. We unfold the iterative algorithm to a so-called Deep Hankel Matrix Factorization network (DHMF). Given the success of the training network using solely synthetic data [12], we also synthesize exponentials and then feed into the network to learn the mapping from the input, i.e. undersampled exponentials, to the output, fully sampled exponentials. Results demonstrate that, compared with the state-of-the-art model-based and DL-based methods, the proposed DHMF is much faster than the former, and is easier to be interpreted than the latter one. Moreover,

DHMF achieves lower reconstruction error than the compared methods and preserves the low-intensity signals much better. Further verifications on the realistic biological NMR spectroscopy also confirms the advantage of the proposed method.

The rest of this paper is organized as follows. Sections II and III introduce mathematical notations and model-based methods, respectively. In Section IV, we propose the method and provide the interpretation of the network structure. Section V elaborates experiments setup and analyze the results. Section VI and VII provides discussions and conclusions.

II. NOTATIONS

We start with the notation used throughout this paper. Scalar x , vector \mathbf{x} , matrix \mathbf{X} and identity matrix \mathbf{I} . The j -th entry of a vector is denoted by \mathbf{x}_j and the (i, j) -th entry of a matrix is \mathbf{X}_{ij} . The notation $\|\cdot\|_p$ represents the standard p -norm, $\|\cdot\|_*$ nuclear norm, and $\|\cdot\|_F$ Frobenius norm. The transpose of vector and matrix are denoted by \mathbf{x}^T and \mathbf{X}^T , while their conjugate transpose is denoted by \mathbf{x}^H and \mathbf{X}^H . \mathbf{X}^{-1} represents the inverse of the matrix \mathbf{X} . Superscript k denotes the number of iterations.

Operators are denoted by calligraphic letters. \mathcal{R} denotes the Hankel operator mapping the vector $\mathbf{x} \in \mathbb{C}^N$ to a Hankel matrix $\mathcal{R}\mathbf{x} \in \mathbb{C}^{N_1 \times N_2}$ with $N_1 + N_2 = N + 1$ as follows:

$$\mathcal{R}: \mathbf{x} \in \mathbb{C}^{N_1+N_2-1} \mapsto \mathbf{X} \in \mathbb{C}^{N_1 \times N_2}, \mathbf{X}_{ij} = \mathbf{x}_{i+j-1}, \quad (2)$$

and the corresponding inverse operator \mathcal{R}^* which turns a Hankel matrix to a vector is given by

$$\mathcal{R}^*: \mathbf{X} \in \mathbb{C}^{N_1 \times N_2} \mapsto \mathbf{x} \in \mathbb{C}^{N_1+N_2-1}, \mathbf{x}_g = \sum_{i+j-1=g} \frac{\mathbf{X}_{ij}}{(\mathcal{R}\mathbf{o})_{ij}}, \quad (3)$$

where $\mathbf{o} \in \mathbb{C}^{N_1+N_2-1}$ is the vector whose elements are all ones, for any $i \in \{1, \dots, N_1\}$ and $j \in \{1, \dots, N_2\}$.

III. RELATED WORK

In this section, we brief review two typical model-based reconstruction methods, including the Low-Rank Hankel Matrix (LRHM) [7] and Low-Rank Hankel Matrix Factorization (LRHMF) [9] and one state-of-the-art deep learning method [12].

LRHM utilizes the low rank property of the Hankel matrix $\mathcal{R}\mathbf{x}$ as a constraint:

$$\min_{\mathbf{x}} \|\mathcal{R}\mathbf{x}\|_* + \frac{\lambda}{2} \|\mathbf{y} - \mathcal{U}\mathbf{x}\|_2^2, \quad (4)$$

where \mathcal{U} denotes the undersampling operator, $\|\mathcal{R}\mathbf{x}\|_*$ is the nuclear norm, defined as the sum of singular values, as an indicator of the matrix rank, $\|\mathbf{y} - \mathcal{U}\mathbf{x}\|_2^2$ is the data consistency term, and the regularization parameter λ tradeoffs between the low rankness and data consistency.

To avoid computing the singular values that usually requires time-consuming SVD, the LRHMF employs a factorization $\mathcal{R}\mathbf{x} = \mathbf{P}\mathbf{Q}^H$ to replace the nuclear norm[37]:

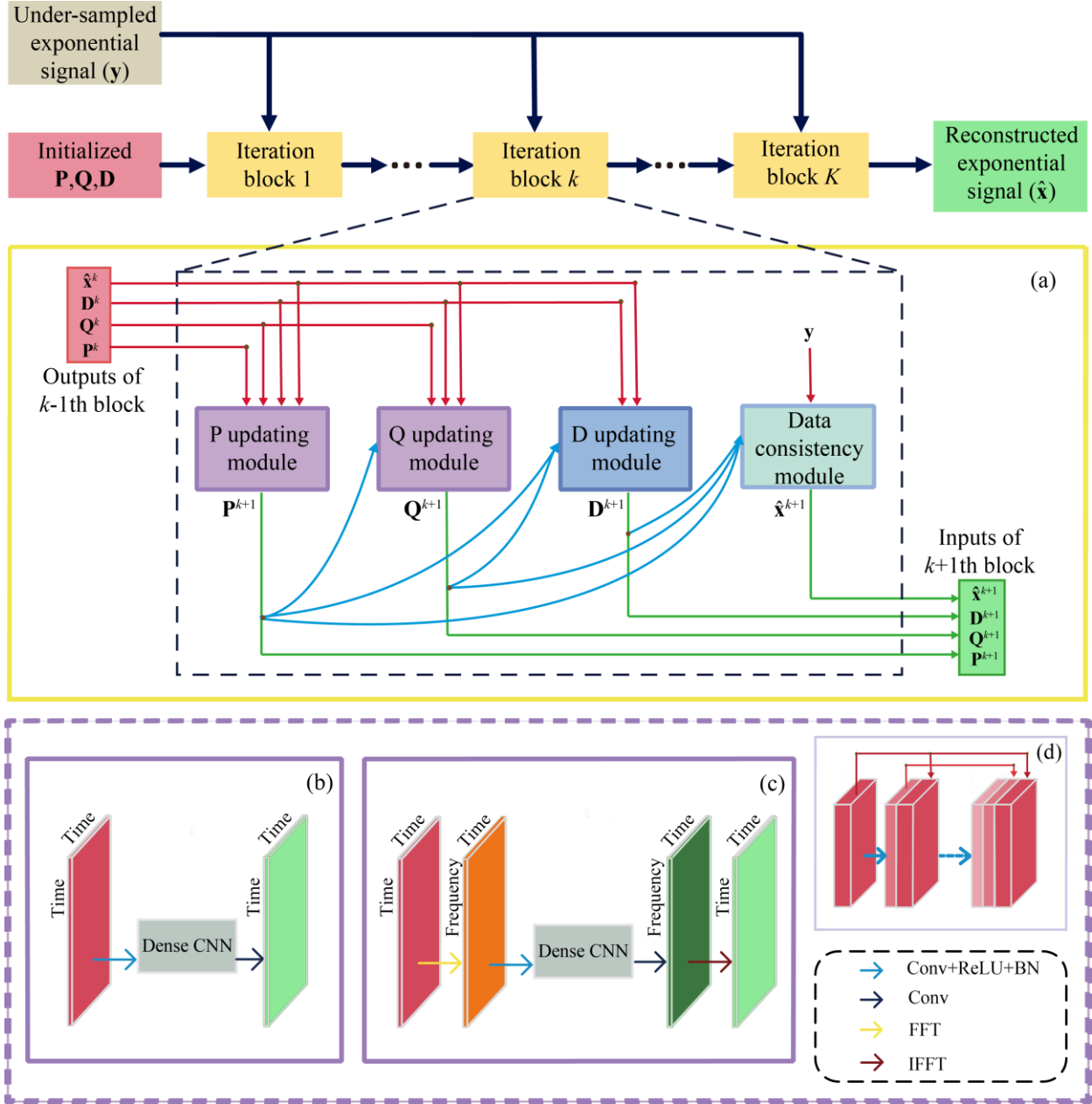


Fig. 2. The architecture of DHMF. (a) the general process of the k -th block, (b) P/Q modules with time domain convolution in the basic DHMF, (c) P/Q modules with frequency domain convolution in the enhanced DHMF, (d) dense convolutional neural network.

$$\| \mathbf{X} \|_* = \min_{\mathbf{P}, \mathbf{Q}} \frac{1}{2} (\| \mathbf{P} \|_F^2 + \| \mathbf{Q} \|_F^2), \text{ s.t. } \mathbf{P} \mathbf{Q}^H = \mathbf{X} \quad (5)$$

where $\mathbf{P} \in \mathbb{C}^{N_t \times R}$ and $\mathbf{Q} \in \mathbb{C}^{N_s \times R}$. Then, equation (4) is reformulated as :

$$\min_{\mathbf{x}, \mathbf{P}, \mathbf{Q}} \frac{1}{2} (\| \mathbf{P} \|_F^2 + \| \mathbf{Q} \|_F^2) + \frac{\lambda}{2} \| \mathbf{y} - \mathcal{U} \mathbf{x} \|_2^2, \text{ s.t. } \mathcal{R} \mathbf{x} = \mathbf{P} \mathbf{Q}^H. \quad (6)$$

The augmented Lagrangian function of (6) is

$$\begin{aligned} L(\mathbf{x}, \mathbf{P}, \mathbf{Q}, \mathbf{D}) = & \frac{1}{2} \| \mathbf{P} \|_F^2 + \frac{1}{2} \| \mathbf{Q} \|_F^2 + \frac{\lambda}{2} \| \mathbf{y} - \mathcal{U} \mathbf{x} \|_2^2 \\ & + \langle \mathbf{D}, \mathcal{R} \mathbf{x} - \mathbf{P} \mathbf{Q}^H \rangle + \frac{\beta}{2} \| \mathcal{R} \mathbf{x} - \mathbf{P} \mathbf{Q}^H \|_F^2 \end{aligned} \quad (7)$$

where \mathbf{D} denotes the augmented Lagrange multiplier, $\langle \cdot, \cdot \rangle$ represents an inner product operator, parameters $\beta > 0$, and

$\beta > 0$ is used to balance between each term. An alternating direction method of multipliers [38] method was introduced to minimize (7) and the solution at the k -th iteration is :

$$\begin{cases} \mathbf{x}^{k+1} = (\lambda \mathcal{U}^* \mathcal{U} + \beta \mathcal{R}^* \mathcal{R})^{-1} (\lambda \mathcal{U}^* \mathbf{y} + \beta \mathcal{R}^* (\mathbf{P}^k (\mathbf{Q}^k)^H - \mathbf{D}^k)) \\ \mathbf{P}^{k+1} = \beta (\mathcal{R} \mathbf{x}^{k+1} + \mathbf{D}^k) \mathbf{Q}^k (\beta (\mathbf{Q}^k)^H \mathbf{Q}^k + \mathbf{I})^{-1} \\ \mathbf{Q}^{k+1} = \beta (\mathcal{R} \mathbf{x}^{k+1} + \mathbf{D}^k)^H \mathbf{P}^{k+1} (\beta (\mathbf{P}^{k+1})^H \mathbf{P}^{k+1} + \mathbf{I})^{-1} \\ \mathbf{D}^{k+1} = \mathbf{D}^k + \tau (\mathcal{R} \mathbf{x}^{k+1} - \mathbf{P}^{k+1} (\mathbf{Q}^{k+1})^H) \end{cases}, \quad (8)$$

where τ is a step size. LRHMF runs much faster and obtains comparable reconstruction errors than LRHM in application [9].

Recently, deep learning has been introduced into exponential signal reconstruction and applied to fast NMR spectroscopy [12]. This method stacks several dense convolution neural networks together and refines the intermediately reconstructed spectra by enforcing data consistency. Then, the spectrum

artifacts in the frequency domain are gradually removed through the dataflow of the network. We call it Deep Learning NMR (DLNMR) throughout the paper. As a proof of concept, most spectra are reconstructed faithfully with a trained neural network from synthetic exponentials. However, small spectral peaks may be distorted or even disappeared; thus, further improvement is expected.

IV. PROPOSED METHOD

In this section, we will propose the Deep Hankel Matrix Factorization (DHMF) neural network and introduce its enhanced version.

A. Basic DHMF

The DHMF unfolds the iterative process of LRHMF[9] into three updating modules \mathbf{P} , \mathbf{Q} , \mathbf{D} and one data consistency module (Fig. 2). Each module corresponds to the updating of four intermediate variables in (8). The four modules constitute a block and the whole network is a stack of K blocks.

1) Updating Module of \mathbf{P} and \mathbf{Q}

Here, the dense convolutional network [39], followed by Rectified Linear Unit (ReLU) and Batch Normalization (BN), is adopted to learn the updating operators \mathcal{P} and \mathcal{Q} because it enables maximum information flow in the network. To leave the historical information of \mathbf{P}^k and \mathbf{Q}^k transfer to the following layers, \mathbf{P} and \mathbf{Q} updating modules of k -th ($k = 1, 2, \dots, K$) block are designed as:

$$\begin{aligned}\mathbf{P}^{k+1} &= \mathcal{P}^k((\mathcal{R}\hat{\mathbf{x}}^k + \mathbf{D}^k)\mathbf{Q}^k, \mathbf{Q}^k, \mathbf{P}^k) \\ \mathbf{Q}^{k+1} &= \mathcal{Q}^k((\mathcal{R}\hat{\mathbf{x}}^k + \mathbf{D}^k)^H \mathbf{P}^{k+1}, \mathbf{P}^{k+1}, \mathbf{Q}^k)\end{aligned}\quad (9)$$

In the implementation, the real and imaginary parts of the input are concatenated together and then separated into two parts of complex variables after updating.

2) Updating Module of \mathbf{D}

The updating module of \mathbf{D} is calculated by:

$$\mathbf{D}^{k+1} = \mathbf{D}^k + \tau(\mathcal{R}\hat{\mathbf{x}}^k - \mathbf{P}^{k+1}(\mathbf{Q}^{k+1})^H), \quad (10)$$

where τ is set as a constant and \mathbf{D} initialized as a zero matrix.

3) Data Consistency Module

Since the time domain signal \mathbf{x} in (8) should be aligned to acquired data [12, 40], the data consistency module is designed as:

$$\hat{\mathbf{x}}^{k+1} = \mathcal{S}(\mathbf{y}, \mathcal{R}^*(\mathbf{P}^{k+1}(\mathbf{Q}^{k+1})^H - \mathbf{D}^{k+1})), \quad (11)$$

where \mathcal{S} denotes the data consistency operator. Let $\hat{\mathbf{x}}^{k+1}$ be the restored data obtained by $\mathcal{R}^*(\mathbf{P}^{k+1}(\mathbf{Q}^{k+1})^H - \mathbf{D}^{k+1})$, equation (11) is equal to the following relationship:

$$\hat{\mathbf{x}}_n^{k+1} = \begin{cases} \hat{\mathbf{x}}_n^{k+1}, & \text{if } n \notin \Omega \\ \frac{\hat{\mathbf{x}}_n^{k+1} + \lambda \mathbf{y}_n}{1 + \lambda}, & \text{if } n \in \Omega \end{cases}, \quad (12)$$

where Ω is the set of positions for sampled exponential signal, n is the index of the signal. Equation (12) implies that the exponential signal at the location of sampled data points should maintain a tradeoff between the sampled data \mathbf{y} and the restored data $\hat{\mathbf{x}}_n^{k+1}$ under a parameter λ .

Overall, time domain convolution networks are trained in \mathbf{P} and \mathbf{Q} updating modules, while in \mathbf{D} updating modules and data consistency modules, variables are directly calculated and no parameter needs to be trained. With the four modules in each block, spectrum artifacts are reduced by increasing the number of blocks, which is similar to the observation in DLNMR [12].

B. Enhanced DHMF

In the basic DHMF, all the convolution is performed in the time domain (Fig. 2(b)). This operation, however, may lose some global information as the convolution kernel is usually not too long. To better explore this information, we first use the fast Fourier transform (FFT) or inverse FFT (IFFT) in the columns of variables \mathbf{P} and \mathbf{Q} and then perform the convolution in the frequency domain (Fig. 2(c)).

As a representative example in Fig. 3. The enhanced DHMF better preserves the low-intensity peaks while the basic DHMF still presents some artifacts. To further evaluate the reconstruction error, we use the Relative Least Normalized Error (RLNE) [10, 11, 15] defined as:

$$\text{RLNE} = \frac{\|\mathbf{x} - \hat{\mathbf{x}}\|_2}{\|\mathbf{x}\|_2}, \quad (13)$$

to measure the difference between the reconstruction $\hat{\mathbf{x}}$ and the noise-free fully sampled signal \mathbf{x} .

In the following parts, we only use enhanced DHMF and call it DHMF for simplicity.

C. Loss Function and Hyper-parameters

Following the most general strategy in deep learning, the sum of the mean squared errors (equation (14)) is chosen as the loss function to measure the difference between the reconstructed signal $\hat{\mathbf{x}}$ and noise-free fully sampled signal \mathbf{x} . Besides, to make the output of each block $\hat{\mathbf{x}}_q^k$ approaches to the ground truth \mathbf{x} , the loss function on $\hat{\mathbf{x}}_q^k(\Theta) - \mathbf{x}_q$ is also constrained. This process was suggested to make the solution steadily approach the solution in previous work[12].

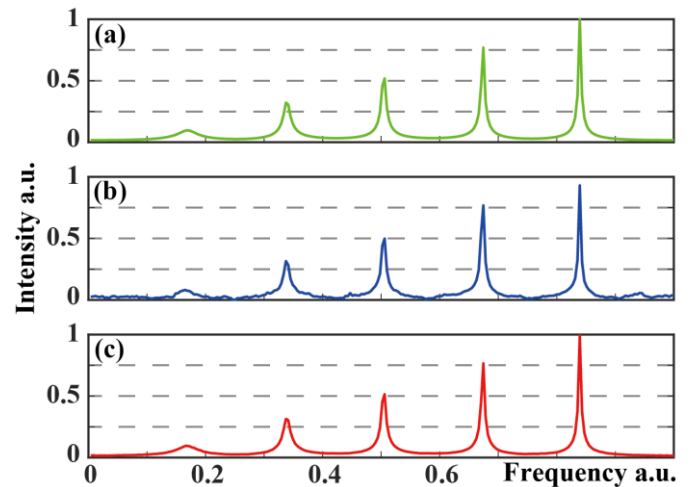


Fig. 3. Reconstructed spectra from undersampled five synthetic exponentials, (a) is the fully sampled signal, (b) and (c) are the reconstructed by basic DHMF and enhanced DHMF, respectively. Note: The length of the fully sampled data is 255 and 25% is acquired. The reconstruction errors, RLNEs, of basic DHMF and enhanced DHMF are 0.1813 and 0.0145, respectively.

TABLE I
PARAMETERS FOR 1D SYNTHETIC EXPONENTIAL SIGNAL

Parameters	Number of exponentials(J)	Amplitude (A)	Normalized frequency(f)	Damping factor(τ)	Phase (ϕ)
Minimum	1	0.05	0	10	0
Increment	1	2.2×10^{-16}	2.2×10^{-16}	2.8×10^{-14}	8.8×10^{-16}
Maximum	10	1	1	179.2	2π

Note: The number of peaks increase from 1 to 10 and length of signal is 255, each subset contains a specific number of peaks and other parameters are acquired uniformly at random using Matlab. Thus, we have 10 subsets and each of them consists 4000 signals. The increment is acquired by calculation the accuracy of the float numbers.

Besides, as the matrix factorization constraint $\mathcal{R}\mathbf{x}=\mathbf{P}\mathbf{Q}^H$ in (6) should be satisfied in the conventional model-based method LRHMF, we also add the square of the Frobenius norm of the matrix $(\mathbf{P}\mathbf{Q}^H - \mathcal{R}\mathbf{x})$ in the loss function.

Overall, the final loss function is

$$\mathcal{L}(\Theta) = \frac{1}{Q} \sum_{q=1}^Q \sum_{k=1}^K (\|\hat{\mathbf{x}}_q^k(\Theta) - \mathbf{x}_q\|_2^2 + \gamma \|\mathbf{P}_q^k(\Theta)\mathbf{Q}_q^k(\Theta)^H - \mathcal{R}\mathbf{x}_q\|_F^2), \quad (14)$$

where Θ is the learnable network parameters, γ is the regularization parameter. Subscript q means the q -th index in training data of the total Q sampling trail. In the implementation, optimal parameters Θ are obtained by minimizing (14) with Adam [41] optimizer.

Hyper-parameters in DHMF is a set of parameters which are not learned by the network but chosen manually. For network structure, the size R of variable \mathbf{P} and \mathbf{Q} is set to 20. The kernel size is 3×3 , the number of the layers is 8, and the block number is 5. The parameter τ in \mathbf{D} module, the λ in the data consistency module, and the regularization parameter γ are set to 10^{-3} , $\sqrt{10}$ and 10^{-2} , respectively. For network training, the learning rate starts from 10^{-3} and gradually reduces to $\sqrt{10} \times 10^{-6}$ when the loss function is no longer significantly reduced.

D. Network Interpretation

To demonstrate the network interpretation of DHMF, we show the intermediate reconstructions and corresponding singular values of each iteration block (Fig. 4). As the block increases, a low-rank solution is gradually obtained by DHMF since the rankness indicator, the nuclear of the solution, decreases steadily (Fig. 4(g)) and finally becomes close to the fully sampled signal. The DLNMR, however, increases the nuclear norm at the final iteration block. In each block(Figs. 3(h)-(l)), the DHMF provides a much better approximation of singular values than DLNMR. At the last block(Fig. 4(l)), DHMF provides very close singular values, although they are not exactly the same, to that of the fully sampled signal. These observations imply that the proposed method provides a better approximation of low rank and better interpretation of the reconstruction in the network.

V. RESULTS

In this section, we evaluate the performance of the proposed DHMF on both synthetic exponential signals and realistic

biological NMR spectroscopy with three state-of-the-art approaches, including LRHM [7], LRHMF [9], and DLNMR [12]. Both LRHM and LRHMF are typical model-based iterative algorithms, and LRHMF is an SVD-free version of LRHM. DLNMR is a state-of-the-art deep learning method for exponential signal reconstruction. The data consistency weight λ is set to $\sqrt{10}$ in DHMF, 10^3 in DLNMR, and $\sqrt{10} \times 10^2$ in both LRHM and LRHMF. All these parameters are optimized for the lowest reconstruction errors.

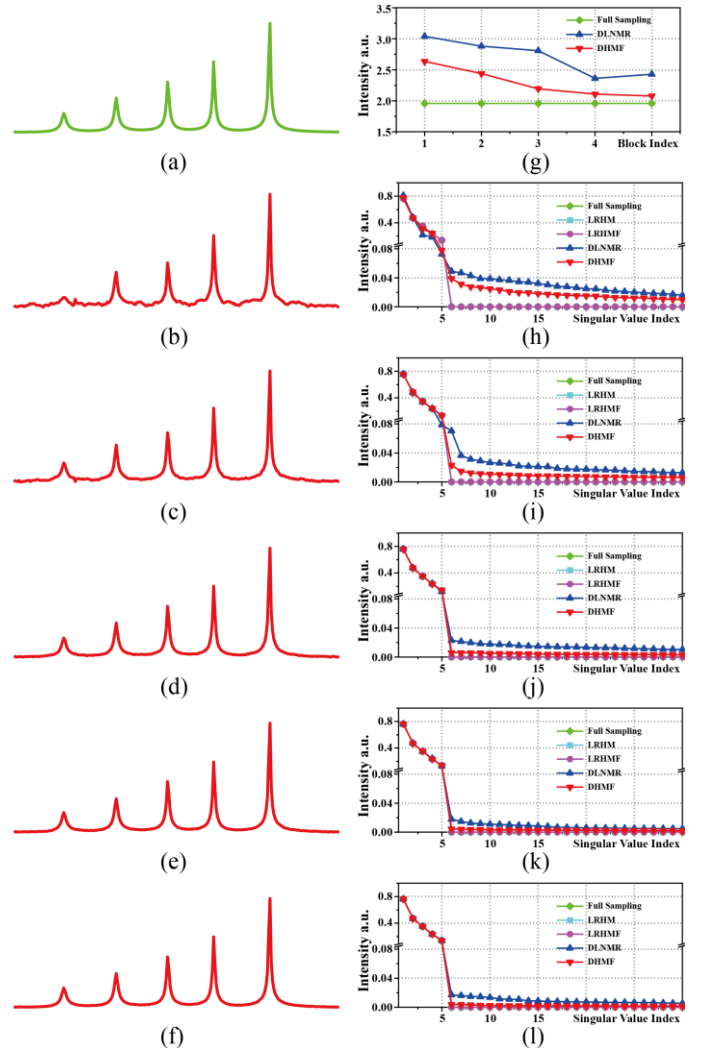


Fig. 4. The reconstructed spectra and singular values at each block. (a) fully sampled spectrum, (b-f) the reconstructed spectrum by the 1st to 5th blocks, (g) the nuclear norm of Hankel matrix of time domain signal, and (h-l) denote corresponding singular values of the output of each block. Note: To show small singular value clearly, there exists a break from 0.084 to 0.085 in Y axis of (h-l).

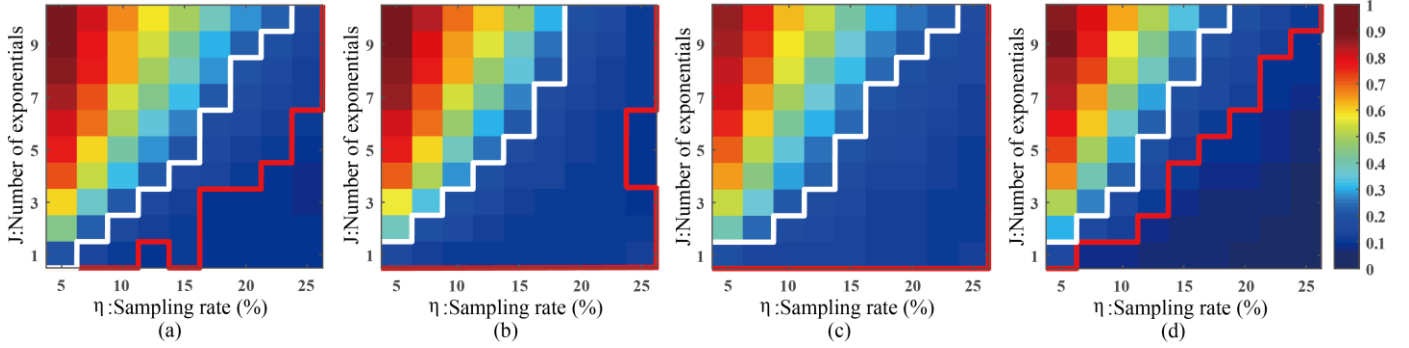


Fig. 5. Average reconstruction error, RLNE, for the synthetic signal. (a) LRHM, (b) LRHMF, (c) DLNMR, (d) DHMF. Note: Each color reflects the average RLNEs over 100 Monte Carlo trials of undersamplings. Red (or white) line indicates an empirical boundary where the threshold of reconstruction error, RLNE, is 0.1 (or 0.2). The reconstruction error in the upper region above (or lower region below) the boundary is greater (or lower) than the threshold. The DLNMR did not obtain any smaller reconstruction error than 0.1 thus the region below the red line is empty. All reconstruction errors are listed in detail in APPENDIX TABLES I-IV.

All experiments were carried out in a computer server equipped with one Intel i9 9900X CPU (3.5 GHz, ten cores), 128 GB RAM, and three NVIDIA RTX 2080Ti GPU cards. The proposed DHMF and DLNMR networks were implemented in python 3.6, using the Keras 2.2.4 package and Tensorflow 1.14.0 as backend. Both LRHM and LRHMF coded in MATLAB (Mathworks Inc.) were parallelized to reduce the computation time under ten CPU cores maximally.

In the following, we use the sampling rate η , which is defined as $\eta = M/N$ where M and N are the number of partially sampled and fully sampled data points. For each fully sampled data points, a corresponding undersampling operator \mathcal{U} is generated following the Poisson-gap sampling scheme[42].

A. Training Data

The network, no matter for the synthetic or realistic data are trained on the same dataset, which solely consists of synthetic exponential signals generated following the parameters in TABLE I. Since the additive Gaussian noise is common in NMR spectroscopy [10-12, 15, 18, 43], the noisy training data is generated according to $\mathbf{y} = \mathcal{U}\mathbf{x} + \delta$ where δ is the Gaussian noise with standard deviation 5×10^{-2} and \mathbf{x} is the noise-free fully sampled exponential signals.

By feeding a signal pair $(\mathbf{y}, \mathcal{U}, \mathbf{x})$ into the network, the learnable parameters of DHMF are optimized until the learning rate decreases to the minimal value $\sqrt{10} \times 10^{-6}$. In the training dataset, a total of $Q=40000$ signal pairs are generated and splits into two parts, including 90% for training and 10% for validation.

B. Reconstruction of Synthetic Data

We first evaluate the reconstruction performance on the synthetic data, which are with different numbers of exponentials, i.e. spectral peaks, and different sampling rates. These data are not presented in the training dataset and generated following (1) with parameters listed in TABLE I.

Reconstruction errors of the synthetic data are shown in Fig. 5. The region below the red line, denoting lower reconstruction error than 0.1, in DHMF is significantly larger than compared methods. Thus, DHMF can reconstruct signals that have a larger number of exponentials or with fewer samples. Among conventional techniques, the LRHM obtains relatively better

reconstruction. However, LRHMF can accelerate LRHM but cannot achieve faithful reconstruction since it is sensitive to an algorithm parameter that is not accessible in practice (See discussions in VI. B). The DLNMR can not commit such a low reconstruction error. As this approach was proposed by our group, this shortcoming motivates us to develop DHMF here. If allowing relatively higher error, e.g. 0.2 marked with white line, LRHM and DLNMR achieve comparable performance while LRHMF allows reconstructing a relatively larger number of exponentials. DHMF still outperforms LRHMF as it enables more exponentials. For example, at the sampling rate 15%, DHMF enables the reconstruction of 8 exponentials, while LRHMF only allows 6 exponentials. These observations imply that DHMF provides better reconstructions than other methods.

A faithful reconstruction of low-intensity peaks is a great challenge in the DL approach [12]. A synthetic signal (Fig. 6(a)), whose spectral intensity of the weakest peak is about 20 times smaller than that of the highest one, is used to evaluate the ability to reconstruct low-intensity peaks. DHMF provides

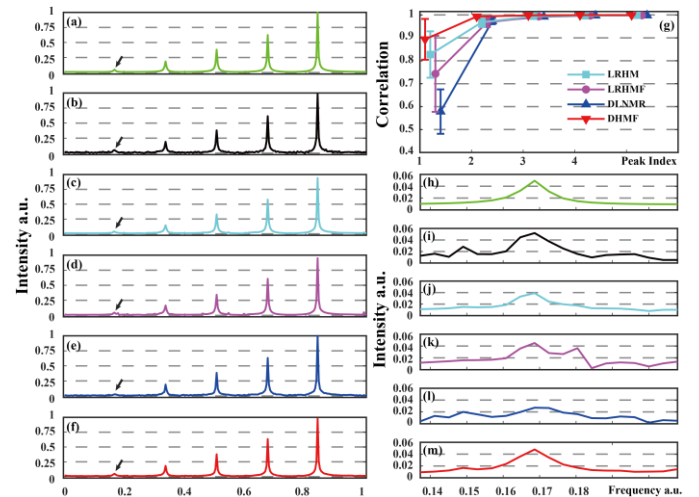


Fig. 6. Reconstructed synthetic signals with low-intensity peaks. (a) is the fully sampled noise-free signal, (b) is the noisy data with the additive Gaussian noise under standard deviation of 0.05, (c-f) are reconstructions obtained by LRHM, LRHMF, DLNMR, and DHMF, respectively, (h-m) are the zoomed in weakest peaks marked by the arrow. (g) is the Pearson's linear correlation coefficient of each peak. Note: The sampling rate is 25%. The average reconstruction error, RLNE, of LRHM, LRHMF, and DLNMR over 100 resampling trials are 0.0991, 0.0963 and 0.0923, respectively, while that of DHMF is only 0.0541.

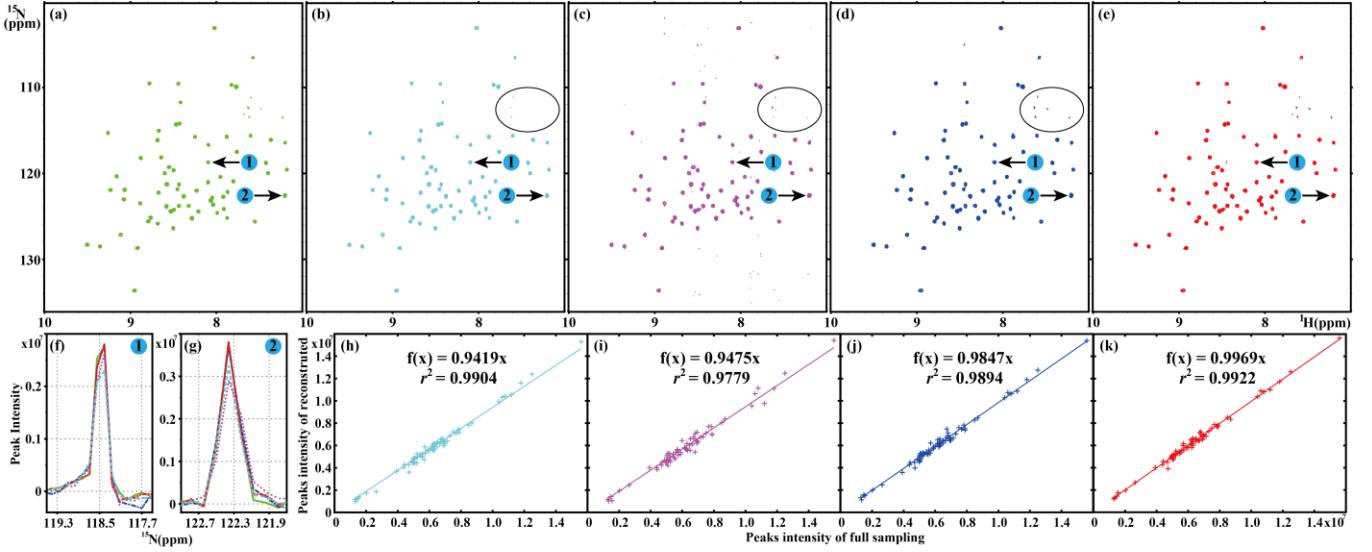


Fig. 7. The reconstruction of 2D ^1H - ^{15}N TROSY spectrum of ubiquitin. (a) is the fully sampled NMR spectrum, (b-e) are the reconstructions by LRHM, LRHMF, DLNMR, and DHMF, respectively. The ppm denotes parts per million by frequency, which is the unit of chemical shift. Gaussian noise with standard deviation 2×10^{-2} is added to the fully sampled spectrum. (f) and (g) are zoomed out 1D ^{15}N traces, (h-k) are peak intensity correlations, and the green, cyan, purple, blue, and red lines represent the spectra obtained with full sampling, LRHM, LRHMF, DLNMR and DHMF, respectively. Note: The regularization parameter λ and rank parameter R in LRHMF are set to 10^2 and 10, respectively. The data size is 127×512 . In NMR, only the indirect dimension is undersampled for fast sampling, while another dimension, called direct dimension, is commonly fully sampled for not time consuming. Here, undersampling is performed on the dimension of 127 at sampling rate 25%.

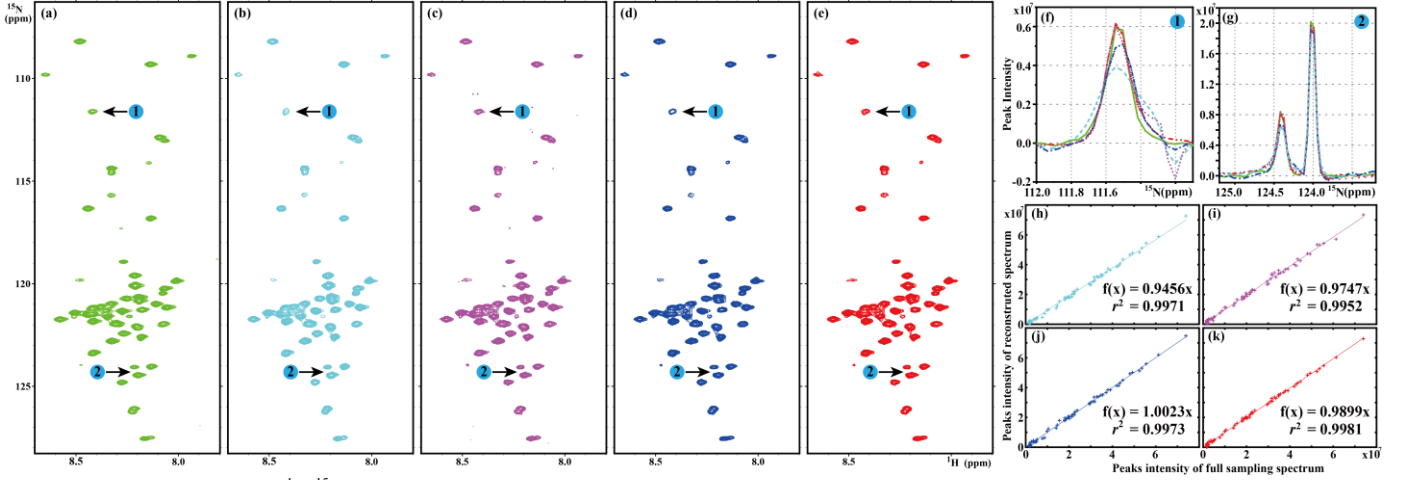


Fig. 8. The reconstruction of 2D ^1H - ^{15}N HSQC spectrum of ubiquitin. (a) is the fully sampled NMR spectrum, (b-e) are the reconstructions by LRHM, LRHMF, DLNMR, and DHMF, respectively. The ppm denotes parts per million by frequency, which is the unit of chemical shift. Gaussian noise with standard deviation 2×10^{-2} is added to the sampled spectrum. (f) and (g) are zoomed out 1D ^{15}N traces, (h-k) are peak intensity correlations, and the green, cyan, purple, blue, and red lines represent the spectra obtained with full sampling, LRHM, LRHMF, DLNMR and DHMF, respectively. Note: The regularization parameter λ and rank parameter R in LRHMF are set to 10^2 and 10, respectively. The data size is 255×116 and the undersampling is performed on the dimension of 255 at sampling rate 25%.

the most consistent spectral peak shape and intensity (Fig. 6(m)) to the fully sampled peak (Fig. 6(h)). DLNMR hardly retrieves the weakest peaks while both LRHM and LRHMF introduce pseudo peak around the ground-truth weak peak. We further measure the peak correlation between reconstructed peaks and corresponding fully sampled noise-free peaks. For the given vectors \mathbf{a} and \mathbf{b} , Pearson's linear correlation coefficient r is defined as:

$$r(\mathbf{a}, \mathbf{b}) = \frac{\sum_{i=1}^n (\mathbf{a}_i - \bar{\mathbf{a}})(\mathbf{b}_i - \bar{\mathbf{b}})}{\sqrt{\sum_{i=1}^n (\mathbf{a}_i - \bar{\mathbf{a}})^2} \sqrt{\sum_{i=1}^n (\mathbf{b}_i - \bar{\mathbf{b}})^2}}, \quad (15)$$

where $\bar{\mathbf{a}}$ and $\bar{\mathbf{b}}$ denotes the mean value of the vectors \mathbf{a} and \mathbf{b} , respectively. The length n for each peak is defined such that the region around the central peak can be almost covered. Fig. 6(g) shows that DHMF significantly possesses the highest correlation on the weakest peak and better performance on another low-intensity peak.

C. Reconstruction of Realistic NMR Spectroscopy Data

NMR spectroscopy is one of the most powerful tools for the analysis of the composition and structure of chemicals and proteins. In NMR signal sampling, time-domain signals are acquired from spectrometers and are usually modeled as the superposition of damped exponential signals [7-11]. For

TABLE II
QUANTATIVE SCORES For ESTIMATED PARAMETERS

Method	Parameters of exponentials			
	Amplitude	Damping factor	Phase	Frequency
LRHM	2.49±0.99	1.94±1.01	2.54±1.01	2.50±1.01
LRHMF	2.54±1.01	2.45±0.96	2.55±1.04	2.60±1.05
DLNMR	2.26±1.12	2.63±1.11	2.29±1.15	2.31±1.14
DHMF	2.71±1.07	2.98±1.04	2.62±1.12	2.59±1.14

Note: Parameter of exponentials are estimated on the reconstructed signals. For each parameter, we provide a score for each method to indicate the relative accuracy among all methods. A method is scored as 4 if it gets the best accuracy, or scored as 3, 2 and 1 if the method takes the second, third and last place among all methods. The number after the notation “±” is the standard deviation over 9000 randomly generated test signals (with different exponential parameters and sampling rates). As an example, we provide the error of estimate parameters for one sampling trail (Appendix Fig. 1) and the corresponding true parameters (Appendix TABLE V).

comparison, one ^1H - ^{15}N TROSY spectrum (Fig. 7(a)) and another ^1H - ^{15}N HSQC spectrum (Fig. 8(a)) are undersampled following Poisson gap sampling[19].

DHMF obtains a faithful recovery while LRHM underestimates the intensity of peaks (Fig. 7(f)(g) and Fig. 8(f)(g)), and LRHMF introduces pseudo peaks (Fig. 7(c) and Fig. 8(c)). Besides, all the compared methods lose weak peaks marked in the black circle (Fig. 7(b-d)), but DHMF does not. The correlation of peak intensity (Fig. 7(h-k) and Fig. 8(h-k)) is also computed for quantitative analysis. The DHMF achieves the highest correlation r among all methods. Therefore, the proposed method provides the most faithful reconstruction for the realistic NMR spectra.

VI. DISCUSSIONS

A. Estimation of Exponential Parameters

We further evaluate the accuracy of parameters of exponentials, including frequency, amplitude, damping factor, and phase, that are retrieved from reconstructions by the ESPRIT [44, 45]. A method will score 4 points if it achieves the best accuracy to the ground-truth parameters among all compared methods and scored 1 point if it obtains the worst one. The scores for each parameter are summarized in TABLE II.

The proposed DHMF achieves the highest scores on the amplitude and damping factor and comparable performance on phase and frequency to the best performance of compared methods. Thus, DHMF preserves the amplitude and damping factor much better in the reconstruction.

B. Robustness of Algorithm Parameters

Discussions on the regularization parameter λ for all methods are given here. The regularization parameter λ is used to maintain the for data consistency to the sampled data points. A smaller λ means the acquired data points are with heavier noise. To test the robustness, we measure the reconstruction errors with λ from 1 to $10^{3.5}$ as shown in Fig. 9. It indicates that the deep learning methods, including DHMF and DLNMR, is more robust than the conventional model-based optimization methods, including the LRHM and LRHMF. Besides, the proposed DHMF achieves lower reconstructed errors than DLNMR under all regularization parameters.

Discussions on the parameter R is essential for matrix factorization methods, including LRHMF and DHMF, which

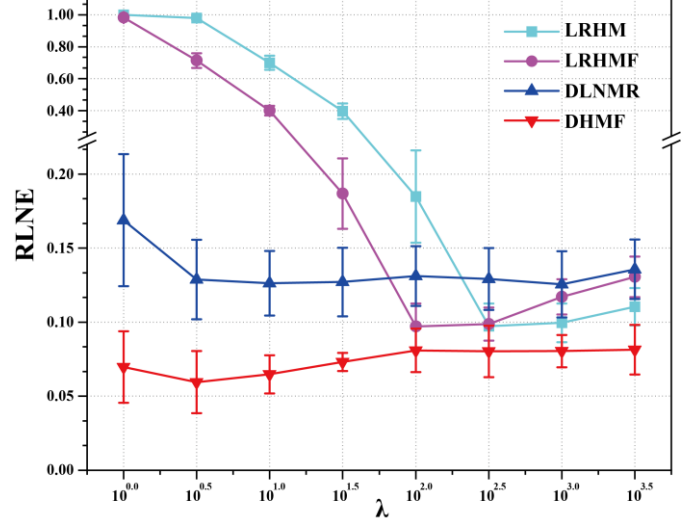


Fig. 9. The regularization parameter λ versus reconstruction errors, RLNEs. Note: The sampling rate is 25% and the error bar stands for the standard deviation under 100 resampling trials. Parameters of the synthetic signal are reported in APPENDIX TABLE VII.

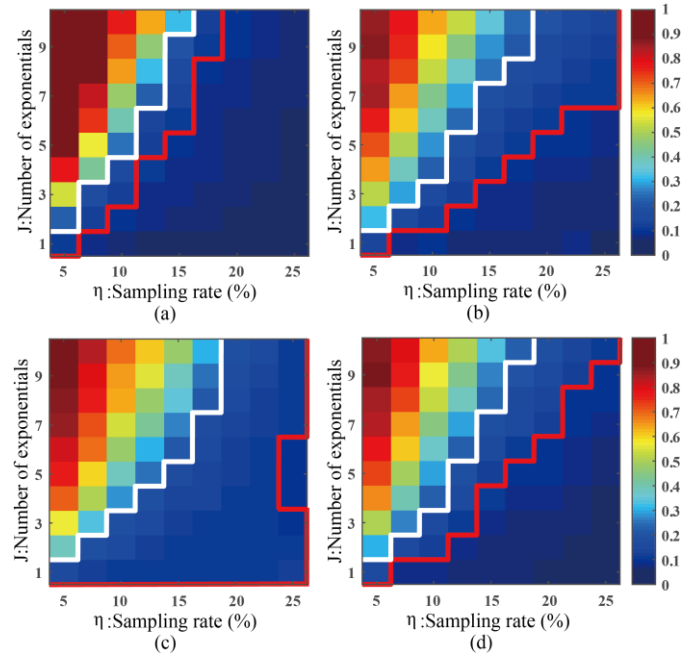


Fig. 10. The average reconstruction errors, RLNEs, for (a)(c) LRHMF with the true rank $R=10$ and empirical setting $R=20$, (b)(d) DHMF with a rank parameter $R=10$ and $R=20$. Note: RLNEs are averaged over 100 Monte Carlo sampling trials.

determines the size of variable \mathbf{P} and \mathbf{Q} , and the upper bound of the rank of $\mathcal{R}\mathbf{x}$, e.g., the number of exponentials in \mathbf{x} . Once the true number of exponentials is known, such as R could be precisely known for synthetic signals, LRHM significantly reduces reconstruction error (Fig. 10(a) than by setting $R=20$ Fig. 10(c)). However, the true R is not accessible in practical undersampling; thus, the performance of LRHM is suboptimal. On the contrary, DHMF does not require the true number of exponentials, e.g., $R=10$ (Fig. 10(b)), and setting R to be much larger, e.g., $R=20$ (Fig. 10(d)), than the true number will and only improve the performance slightly. Thus, DHMF is easy to be used in practice.

C. Computational Time for Reconstructions

One of the advantages of DL is that it can accelerate the reconstruction process by utilizing massive parallel computing of graphic processing units (GPUs) through low complexity neural network algorithms. Though the training stage of the network is time-consuming, this process only needs to be performed once. For a trained network, its reconstruction is much faster than traditional iterative methods, as shown in TABLE III. DHMF costs longer computation time than the state-of-the-art DL method because of the 2D convolution on the Hankel matrix.

TABLE III
COMPUTATIONAL TIME (UNIT: SECOND)

Method \ Size	255	511	1023
LRHM	1.33	5.05	40.13
LRHMF	1.04	8.56	44.35
DLNMR	0.03	0.04	0.06
DHMF	0.39	1.20	5.31

VII. CONCLUSION

In this work, we propose a new deep learning neural network called DHMF by unrolling the model-based matrix factorization for exponential signal recovery. Experimental results on synthetic data and real biological data demonstrate that the DHMF outperforms state-of-the-art model-based and deep learning-based methods on preserving low-intensity signals and obtains more accurate estimation on the amplitude and damping factor of exponentials.

VIII. ACKNOWLEDGMENTS

The authors would like to thank V. Orekhov and M. Mayzel for sharing the NMR data and the GPU donated by NVIDIA Corporation.

APPENDIX

A. Parameter Estimation of Random Synthetic Signal

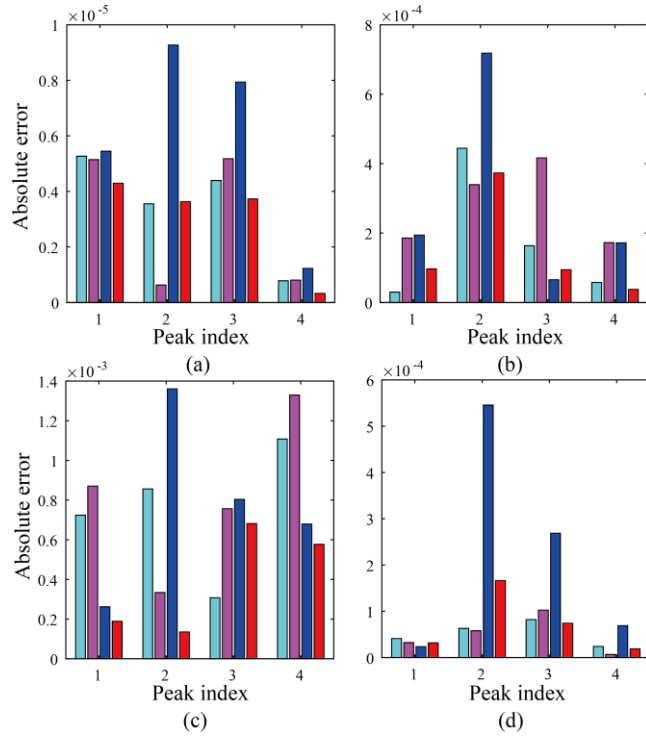


Fig.1 The error of estimated parameters from reconstructions of one random undersampling. (a)-(d) denote the errors of estimated frequency, amplitude, damping factor and phase, respectively. The cyan, purple, blue, and red color correspond to the LRHM, LRHMF, DLNMR, and DHMF method, respectively. Note: True parameters of the signal are listed in APPENDIX TABLE V.

B. Reconstruction Errors

TABLE I
AVERAGE RECONSTRUCTION ERRORS, RLNES, IN LRHM

SR J	5%	7.5%	10%	12.5%	15%	17.5%	20%	22.5%	25%
10	0.883	0.809	0.663	0.586	0.482	0.381	0.282	0.220	0.161
9	0.887	0.780	0.634	0.540	0.424	0.310	0.228	0.183	0.137
8	0.864	0.762	0.631	0.485	0.377	0.272	0.196	0.144	0.123
7	0.846	0.712	0.540	0.431	0.312	0.216	0.167	0.130	0.114
6	0.801	0.684	0.504	0.343	0.260	0.166	0.140	0.114	0.099
5	0.765	0.599	0.411	0.275	0.201	0.146	0.118	0.106	0.093
4	0.708	0.533	0.312	0.214	0.150	0.126	0.108	0.094	0.085
3	0.595	0.375	0.210	0.151	0.122	0.098	0.088	0.087	0.079
2	0.434	0.220	0.156	0.121	0.104	0.097	0.089	0.087	0.085
1	0.203	0.133	0.110	0.098	0.100	0.097	0.094	0.092	0.098

TABLE II
AVERAGE RECONSTRUCTION ERRORS, RLNES, IN LRHMF

SR J	5%	7.5%	10%	12.5%	15%	17.5%	20%	22.5%	25%
10	0.896	0.833	0.691	0.609	0.476	0.309	0.184	0.141	0.109
9	0.904	0.793	0.653	0.554	0.388	0.245	0.165	0.127	0.104
8	0.876	0.769	0.635	0.472	0.337	0.207	0.148	0.118	0.102
7	0.854	0.718	0.535	0.416	0.260	0.176	0.137	0.112	0.104
6	0.802	0.691	0.472	0.301	0.217	0.140	0.121	0.107	0.096
5	0.763	0.589	0.376	0.245	0.173	0.135	0.116	0.108	0.096
4	0.694	0.504	0.277	0.187	0.135	0.126	0.111	0.101	0.095
3	0.565	0.331	0.186	0.140	0.120	0.106	0.101	0.100	0.093
2	0.380	0.187	0.145	0.122	0.110	0.108	0.104	0.103	0.102
1	0.153	0.115	0.107	0.101	0.108	0.107	0.106	0.104	0.112

TABLE III
AVERAGE RECONSTRUCTION ERRORS, RLNES, IN DLNMR

SR J	5%	7.5%	10%	12.5%	15%	17.5%	20%	22.5%	25%
10	0.853	0.843	0.620	0.528	0.405	0.300	0.253	0.204	0.174
9	0.843	0.735	0.579	0.482	0.350	0.268	0.215	0.179	0.151
8	0.824	0.701	0.558	0.414	0.317	0.240	0.190	0.152	0.138
7	0.808	0.648	0.484	0.362	0.263	0.199	0.173	0.141	0.125
6	0.750	0.610	0.424	0.305	0.242	0.165	0.154	0.133	0.113
5	0.695	0.519	0.346	0.252	0.197	0.157	0.140	0.124	0.105
4	0.648	0.451	0.294	0.221	0.169	0.138	0.130	0.112	0.105
3	0.529	0.359	0.216	0.170	0.138	0.121	0.113	0.111	0.103
2	0.390	0.231	0.169	0.144	0.128	0.115	0.115	0.109	0.108
1	0.190	0.133	0.134	0.125	0.134	0.117	0.118	0.108	0.119

TABLE IV
AVERAGE RECONSTRUCTION ERRORS, RLNES, IN DHMF

SR J	5%	7.5%	10%	12.5%	15%	17.5%	20%	22.5%	25%
10	0.874	0.890	0.632	0.504	0.332	0.224	0.189	0.127	0.107
9	0.890	0.759	0.573	0.440	0.262	0.196	0.148	0.114	0.093
8	0.844	0.722	0.525	0.377	0.233	0.162	0.134	0.096	0.087
7	0.836	0.651	0.446	0.285	0.181	0.138	0.116	0.087	0.078
6	0.781	0.602	0.366	0.228	0.164	0.104	0.095	0.079	0.067
5	0.719	0.491	0.294	0.181	0.120	0.098	0.087	0.076	0.061
4	0.659	0.390	0.222	0.140	0.100	0.085	0.076	0.065	0.057
3	0.503	0.259	0.150	0.104	0.078	0.070	0.064	0.059	0.050
2	0.299	0.146	0.117	0.081	0.070	0.065	0.060	0.053	0.051
1	0.138	0.078	0.076	0.065	0.063	0.059	0.058	0.049	0.046

C. Parameters of Synthetic Signals

TABLE V
SYNTHETIC DATA WITH FOUR PEAKS FOR APPENDIX FIG.1

Peaks ID Parameters	1	2	3	4
Amplitude (A)	0.717	1.000	0.601	0.454
Damping factor (τ)	173.24	126.44	31.59	107.82
Phase (ϕ)	3.5281	5.6890	2.1928	3.8518
Frequency (f)	0.0706	0.1534	0.4166	0.4833

TABLE VI
SYNTHETIC DATA WITH FIVE PEAKS FOR FIG.6 .

Peaks ID Parameters	1	2	3	4	5
Amplitude (A)	0.100	0.300	0.500	0.700	1.000
Damping factor (τ)	50	75	100	125	150
Phase (ϕ)	0	0	0	0	0
Frequency (f)	0.1655	0.3349	0.5004	0.6698	0.8353

TABLE VII
SYNTHETIC DATA WITH FIVE PEAKS FOR FIG.3, FIG.4 and FIG.9.

Peaks ID Parameters	1	2	3	4	5
Amplitude (A)	0.5145	0.6623	0.7253	0.7825	0.9872
Damping factor (τ)	26.47	35.63	48.78	61.51	81.50
Phase (ϕ)	$2\pi/5$	$4\pi/5$	$6\pi/5$	$8\pi/5$	2π
Frequency (f)	0.1532	0.3135	0.4716	0.6124	0.7831

REFERENCES

- [1] A. Hirose and S. Yoshida, "Generalization characteristics of complex-valued feedforward neural networks in relation to signal coherence," *IEEE Trans. Neural Netw. Learn. Syst.*, vol. 23, no. 4, pp. 541-551, 2012.
- [2] C. Qian, L. Huang, M. Cao, J. Xie, and H. C. So, "PUMA: An improved realization of MODE for DOA estimation," *IEEE Trans. Aerosp. Electron. Syst.*, vol. 53, no. 5, pp. 2128-2139, 2017.
- [3] D. Nion and N. D. Sidiropoulos, "Tensor algebra and multidimensional harmonic retrieval in signal processing for mimo radar," *IEEE Trans. Signal Process.*, vol. 58, no. 11, pp. 5693-5705, 2010.
- [4] L. Schermelleh, R. Heintzmann, and H. Leonhardt, "A guide to super-resolution fluorescence microscopy," *J. Cell Biol.*, vol. 190, no. 2, pp. 165-175, 2010.
- [5] J. A. Tropp, J. N. Laska, M. F. Duarte, J. K. Romberg, and R. G. Baraniuk, "Beyond Nyquist: Efficient sampling of sparse bandlimited signals," *IEEE Trans. Inf. Theory*, vol. 56, no. 1, pp. 520-544, 2010.
- [6] M. Vetterli, P. Marziliano, and T. Blu, "Sampling signals with finite rate of innovation," *IEEE Trans. Signal Process.*, vol. 50, no. 6, pp. 1417-1428, 2002.
- [7] X. Qu, M. Mayzel, J.-F. Cai, Z. Chen, and V. Orekhov, "Accelerated NMR spectroscopy with low-rank reconstruction," *Angew. Chem.-Int. Edit.*, vol. 54, no. 3, pp. 852-854, 2015.
- [8] H. M. Nguyen, X. Peng, M. N. Do, and Z.-P. Liang, "Denoising MR spectroscopic imaging data with low-rank approximations," *IEEE Trans. Biomed. Eng.*, vol. 60, no. 1, pp. 78-89, 2013.
- [9] D. Guo, H. Lu, and X. Qu, "A fast low rank Hankel matrix factorization reconstruction method for non-uniformly sampled magnetic resonance spectroscopy," *IEEE Access*, vol. 5, pp. 16033-16039, 2017.
- [10] J. Ying, H. Lu, Q. Wei, J.-F. Cai, D. Guo, J. Wu, Z. Chen, and X. Qu, "Hankel matrix nuclear norm regularized tensor completion for N-dimensional exponential signals," *IEEE Trans. Signal Process.*, vol. 65, no. 14, pp. 3702-3717, 2017.
- [11] H. Lu, X. Zhang, T. Qiu, J. Yang, J. Ying, D. Guo, Z. Chen, and X. Qu, "Low rank enhanced matrix recovery of hybrid time and frequency data in fast magnetic resonance spectroscopy," *IEEE Trans. Biomed. Eng.*, vol. 65, no. 4, pp. 809-820, 2018.
- [12] X. Qu, Y. Huang, H. Lu, T. Qiu, D. Guo, T. Agback, V. Orekhov, and Z. Chen, "Accelerated nuclear magnetic resonance spectroscopy with deep learning," *Angew. Chem.-Int. Edit.*, vol. 59, no. 26, pp. 10297-10300, 2020.
- [13] K. Usevich and P. Comon, "Hankel low-rank matrix completion: Performance of the nuclear norm relaxation," *IEEE J. Sel. Top. Signal Process.*, vol. 10, no. 4, pp. 637-646, 2016.
- [14] Y. Chen and Y. Chi, "Robust spectral compressed sensing via structured matrix completion," *IEEE Trans. Inf. Theory*, vol. 60, no. 10, pp. 6576-6601, 2014.
- [15] J. Ying, J.-F. Cai, D. Guo, G. Tang, Z. Chen, and X. Qu, "Vandermonde factorization of hankel matrix for complex exponential signal recovery—application in fast nmr spectroscopy," *IEEE Trans. Signal Process.*, vol. 66, no. 21, pp. 5520-5533, 2018.
- [16] K. Kazimierzczuk and V. Y. Orekhov, "Accelerated NMR spectroscopy by using compressed sensing," *Angew. Chem.-Int. Edit.*, vol. 50, no. 24, pp. 5556-5559, 2011.
- [17] X. Qu, X. Cao, D. Guo, and Z. Chen, "Compressed sensing for sparse magnetic resonance spectroscopy," in *Int. Soc. Magn. Reson. Med. 18th Sci. Meet.*, 2010, p. 3371.
- [18] D. J. Holland, M. J. Bostock, L. F. Gladden, and D. Nietlispach, "Fast multidimensional NMR spectroscopy using compressed sensing," *Angew. Chem.-Int. Edit.*, vol. 50, no. 29, pp. 6548-6551, 2011.
- [19] S. G. Hyberts, K. Takeuchi, and G. Wagner, "Poisson-gap sampling and forward maximum entropy reconstruction for enhancing the resolution and sensitivity of protein NMR data," *J. Am. Chem. Soc.*, vol. 132, no. 7, pp. 2145-2147, 2010.
- [20] X. Qu, D. Guo, X. Cao, S. Cai, and Z. Chen, "Reconstruction of self-sparse 2d NMR spectra from undersampled data in the indirect dimension," *Sensors*, vol. 11, no. 9, pp. 8888-8909, 2011.
- [21] Z. Tu, H. Liu, J. Zhan, and D. Guo, "A fast self-learning subspace reconstruction method for non-uniformly sampled nuclear magnetic resonance spectroscopy," *Appl. Sci.-Basel*, vol. 10, no. 11, p. 3939, 2020.
- [22] E. J. Candès, J. Romberg, and T. Tao, "Robust uncertainty principles: Exact signal reconstruction from highly incomplete frequency information," *IEEE Trans. Inf. Theory*, vol. 52, no. 2, pp. 489-509, 2006.
- [23] V. Chandrasekaran, B. Recht, P. A. Parrilo, and A. S. Willsky, "The convex geometry of linear inverse problems," *Found. Comput. Math.*, vol. 12, no. 6, pp. 805-849, 2012.
- [24] M. Fazel, T. K. Pong, D. Sun, and P. Tseng, "Hankel matrix rank minimization with applications to system identification and realization," *SIAM J. Matrix Anal. Appl.*, vol. 34, no. 3, pp. 946-977, 2013.
- [25] I. Markovsky, "Recent progress on variable projection methods for structured low-rank approximation," *Signal Process.*, vol. 96, pp. 406-419, 2014.
- [26] J.-F. Cai, X. Qu, W. Xu, and G. Ye, "Robust recovery of complex exponential signals from random Gaussian projections via low rank Hankel matrix reconstruction," *Appl. Comput. Harmon. Anal.*, vol. 41, no. 2, pp. 470-490, 2016.
- [27] I. Markovsky and K. Usevich, "Structured low-rank approximation with missing data," *SIAM J. Matrix Anal. Appl.*, vol. 34, no. 2, pp. 814-830, 2013.
- [28] X. Peng, C. Lu, Z. Yi, and H. Tang, "Connections between nuclear-norm and Frobenius-norm-based representations," *IEEE Trans. Neural Netw. Learn. Syst.*, vol. 29, no. 1, pp. 218-224, 2018.
- [29] J.-F. Cai, E. J. Candès, and Z. Shen, "A singular value thresholding algorithm for matrix completion," *SIAM J. Optim.*, vol. 20, no. 4, pp. 1956-1982, 2010.
- [30] K. H. Jin, D. Lee, and J. C. Ye, "A general framework for compressed sensing and parallel MRI using annihilating filter based low-rank Hankel matrix," *IEEE Trans. Comput. Imaging*, vol. 2, no. 4, pp. 480-495, 2016.
- [31] X. Zhang, D. Guo, Y. Huang, Y. Chen, L. Wang, F. Huang, Q. Xu, and X. Qu, "Image reconstruction with low-rankness and self-consistency of k-space data in parallel MRI," *Med. Image Anal.*, vol. 63, p. 101687, 2020.
- [32] Y. LeCun, Y. Bengio, and G. Hinton, "Deep learning," *Nature*, vol. 521, no. 7553, pp. 436-444, 2015.
- [33] R. Liu, Z. Jiang, X. Fan, and Z. Luo, "Knowledge-driven deep unrolling for robust image layer separation," *IEEE Trans. Neural Netw. Learn. Syst.*, vol. 31, no. 5, pp. 1653-1666, 2020.
- [34] D. Chen, Z. Wang, D. Guo, V. Orekhov, and X. Qu, "Review and prospect: Deep learning in nuclear magnetic resonance spectroscopy," *Chem.-Eur. J.*, vol. 26, pp. 10391-10401, 2020.
- [35] Y. Yang, J. Sun, H. Li, and Z. Xu, "ADMM-CSNet: A deep learning approach for image compressive sensing," *IEEE Trans. Pattern Anal. Mach. Intell.*, vol. 42, pp. 521-538, 2020.
- [36] T. Lu, X. Zhang, Y. Huang, D. Guo, F. Huang, Q. Xu, Y. Hu, L. Ou-Yang, J. Lin, and Z. Yan, "pFISTA-SENSE-ResNet for parallel MRI reconstruction," *J. Magn. Reson.*, vol. 318, p. 106790, 2020.
- [37] N. Srebro, "Learning with matrix factorizations," Ph.D. thesis, 2004.
- [38] S. Boyd, N. Parikh, E. Chu, B. Peleato, and J. Eckstein, "Distributed optimization and statistical learning via the alternating direction method of multipliers," *Found. Trends Mach. Learn.*, vol. 3, no. 1, pp. 1-122, 2011.
- [39] G. Huang, Z. Liu, L. Van Der Maaten, and K. Q. Weinberger, "Densely connected convolutional networks," in *Proc. IEEE Comput. Soc. Conf. Comput. Vision Pattern Recognit.*, 2017, pp. 4700-4708.
- [40] W. Lee, M. Tonelli, and J. L. Markley, "NMRFAM-SPARKY: Enhanced software for biomolecular NMR spectroscopy," *Bioinformatics*, vol. 31, no. 8, pp. 1325-1327, 2015.
- [41] D. P. Kingma and J. Ba, "Adam: A method for stochastic optimization," *arXiv Preprint arXiv:1412.6980*, 2014.
- [42] F. Delaglio, S. Grzesiek, G. W. Vuister, G. Zhu, J. Pfeifer, and A. Bax, "NMRPipe: A multidimensional spectral processing system based on UNIX pipes," *J. Biomol. NMR*, vol. 6, no. 3, pp. 277-293, 1995.
- [43] J. C. Hoch and A. S. Stern, *NMR Data Processing*. 1996.
- [44] R. Roy and T. Kailath, "ESPRIT-estimation of signal parameters via rotational invariance techniques," *IEEE Trans. Acoust., Speech, Signal Process.*, vol. 37, no. 7, pp. 984-995, 1989.
- [45] P. Stoica and R. L. Moses, *Spectral analysis of signals*. Prentice-Hall, Upper Saddle River, Nj, 2005.